

# Optical Detection of Star Formation in a Cold Dust Cloud in the Counterjet Direction of Centaurus A

William C. Keel<sup>1</sup>

*Department of Physics and Astronomy, University of Alabama, Box 870324, Tuscaloosa, AL 35487*

wkeel@ua.edu

and

Julie K. Banfield and Anne Medling<sup>2,3</sup>

*Research School of Astronomy and Astrophysics, Australian National University, Canberra, ACT 2611, Australia*

and

Susan G. Neff

*NASA Goddard Space Flight Center*

## ABSTRACT

We have identified a set of optical emission-line features  $700''$  (12 kpc) to the southwest of the nucleus of Centaurus A, roughly opposite to the radio jet and well-known optical emission filaments associated with the northern radio structure (along the axis of the southwestern radio lobes, although there is no coherent counterjet at this radius). We use integral-field optical spectroscopy to trace the ratios of strong emission lines, showing changes in excitation across the region, and significant local reddening. The emission regions are spatially associated with far-infrared emission peaks in one of two cold dust clouds identified using *Herschel* and *Spitzer* data, and there may be a mismatch between the low temperature of the dust and the expected heating effect of young stars. The strong emission lines have ratios consistent with photoionization in normal H II regions, requiring only modest numbers of OB stars; these stars and their cooler accompanying populations must be obscured along our line of sight. These data fit with a picture of fairly ordinary formation of clusters in a large giant molecular cloud, or network of such clouds. The location, projected near the radio-source axis and within the radius where a starburst wind has been inferred on the other side of the galaxy, raises the question of whether this star-forming episode was enhanced or indeed triggered by an outflow from the central parts of Centaurus A. However, optical emission-line ratios and line widths limit the role of shocks on the gas, so any interaction with an outflow, associated either with the radio source or star formation in the gas-rich disk of Centaurus A, can at most have compressed the gas weakly. We speculate that the presence of similar star-forming regions on both sides of the galaxy, contrasted with the difference in the character of the emission-line clouds, reflects the presence of a collimated radio jet to the northeast and perhaps anisotropic escape of ionizing radiation from the AGN as well. In this view, the star formation on the southwestern side of Cen A could be enhanced by a broad outflow (whether originated by a starburst or AGN), distinct from the radio jet and lobes.

*Subject headings:* galaxies: individual (NGC 5128) — galaxies: star formation — galaxies: active

## 1. Introduction

Centaurus A (NGC 5128), as the nearest galaxy hosting a large double radio source, has long played a special role in our understanding of similar objects. It displays a host of characteristic features observable in unique detail - a large-scale double source spanning 600 kpc, radio and X-ray jets on scales up to 3 kpc, merger signatures in stars, gas, and dust, and optical emission-line features often attributed to interaction between the propagating jet and ambient interstellar medium, generating both shock ionization and star formation.

Optical emission regions and possible young stars near the northeastern radio jet were identified by Blanco et al. (1975); spectroscopy by Osmer (1978) confirmed that both normal H II region and bright supergiants were present. Graham & Price (1981) used higher-resolution spectra to show that large “turbulent” velocities in the range  $400 \text{ km s}^{-1}$  appear across few-arcsecond scales, well beyond what could be produced in star-forming regions. Data presented by Peterson et al. (1975) show that multiple ionizing mechanisms may be at work, with line ratios in some parts of the first-discovered emission regions have [O I] too strong for ordinary H II regions ionized by stars. The ionization of the gas in these filaments is complex; Morganti et al. (1991) suggest a dominant role for photoionization by the beamed continuum of a small scale jet. In contrast, Sutherland et al. (1993) present models showing that the small-scale velocity structure matches shock excitation of the spectral lines; *Chandra* X-ray data analyzed by Evans & Koratkar (2004) support this through showing very hot gas along one side of the most prominent filament. Rejkuba et al. (2002) used color-magnitude diagrams to identify local young supergiant stars; comparison of their locations to the ionized gas structure provides additional evidence for multiple ionizing mechanisms, while a deeper *Hubble Space Telescope* analysis by Crockett et al. (2012) makes this case more

stringently in the brightest emission region.

Santoro et al. (2015) show that the dynamics of ionized gas in the prominent filaments are consistent with the ambient H I clouds, including components in regular rotation about the galaxy as well as being entrained by the radio jet. Additional MUSE observations by Santoro et al. (2016) show that even on small scales in these filaments, there is a changing mix of ionization mechanisms, with embedded star formation and photoionization by the distant AGN both indicated by emission-line ratios. McKinley et al. (2017) suggest that one of the outermost emission-line filaments may result from interaction with a wind rather than a collimated jet, and speculate that the southwestern jet may not intersect suitable cold gas to produce similar effects in the “counterjet” direction.

As part of a study of these emission features, we have found an emission-line feature along the “counterjet” direction, which seems to have been previously unremarked<sup>1</sup>. We present here morphological and spectroscopic observations of this object, which appears to consist of (possibly multiple) H II regions powered by young stars. The H $\alpha$  emission is spatially coincident with the peaks of the cold dust feature found by Auld et al. (2012) from *Herschel* observations, furnishing an interesting puzzle as to how a star-forming region coexists with the dust without generating a higher temperature than observed.

The radio structure does not have a distinct counterpart to the northern jet on the southern side at this distance. The regions we observe fall in a minimum in radio flux between inner and outer lobes (Junkes et al. 1993), making direct interaction with a jet unlikely.

In computing sizes and luminosities, we adopt a distance 3.7 Mpc (scale  $17.9 \text{ pc arcsecond}^{-1}$ ), following the Cepheid results of Tully et al. (2013) and the red-giant studies from, e.g., Crnojević et al. (2013) and Tully et al. (2015).

---

<sup>1</sup>As this study was in progress, we found that the emission feature appears in the long-exposure, very deep composite image presented by Rolf Olsen at <http://www.rolfolsenastrophotography.com/Astrophotography/Centaurus-A-Extr> and is described in his text as possibly related to the jet: “A corresponding faint trace of nebulosity, likely related to the otherwise invisible Southern jet, is also noticeable as a small red smudge on the opposite side of the galaxy core”.

---

<sup>1</sup>SARA Observatory

<sup>2</sup>Current address: Cahill Center for Astronomy & Astrophysics, California Institute of Technology, MS 249-17, Pasadena, CA 91125, USA

<sup>3</sup>Hubble Fellow

## 2. Observations

### 2.1. Identification and optical imaging

The emission region was identified in May 2014 using an  $H\alpha$  filter of FWHM  $75 \text{ \AA}$  on the remotely-operated SARA 0.6m telescope at Cerro Tololo, Chile (Keel et al. 2017). A CCD system from ARC of San Diego operated at  $-110 \text{ C}$ ; the pixel scale was  $0.38''$ . We coadded images totaling 7 hours' integration in this filter, and 70 minutes of continuum imaging in the R band, obtained between May and August 2014. Flux calibration used Landolt (2009) standard stars, carried to the narrow filter using the ratio of filter widths. The narrowband image (Fig. 1) shows a set of diffuse  $H\alpha$  emission regions, and two starlike objects with strong residual  $H\alpha$  flux after continuum subtraction using the  $R$  image. Color terms in this subtraction will be modest, because  $H\alpha$  is near the center of the  $R$  band. The image gives a total  $H\alpha + [\text{N II}]$  flux within the brightest  $15 \times 15''$  region of  $6.1 \times 10^{-15} \text{ erg cm}^{-2} \text{ s}^{-1} \text{ \AA}^{-1}$ , about 50% lower than implied by the flux calibration of the integral-field spectroscopic data.

For comparison, we also make use of a similar  $H\alpha/R$  image pair centered on the core of Centaurus A, summing total exposures of 4 hours in  $H\alpha$  and 50 minutes in  $R$ , and  $H\alpha$  and  $I$  images of a location in the northeast emission filaments obtained in February 1987 using the ESO/MPI 2.2m telescope at La Silla, as described by Keel (1989)

Coordinates were derived using the astrometry.net Web service (Lang et al. 2010), automatically matching field stars to coordinate catalogs. The emission-line features span an extreme length of  $26''$  (460 pc) in projection; J2000 coordinates are given in Table 1. This region lies 12 kpc in projection from the core of Centaurus A.

### 2.2. Optical spectroscopy

Data cubes in both blue and red grating settings were obtained using the WiFeS integral-field spectrograph (Dopita et al. 2007) at the 2.3m ANU Advanced Technology Telescope at Siding Spring. The field of view spans  $25 \times 38''$ , with  $1''$  sampling. Simultaneous exposures in the blue (3500-5700  $\text{\AA}$ ) and red (5400-7000  $\text{\AA}$ ) ranges were obtained on 4 March 2016, for 900 seconds. The field covered the three southern discrete compo-

nents, as well as more diffuse emission to their northeast, and the southern edge of the NE component.

Strong, narrow emission lines appear; the mean heliocentric radial velocity is  $cz = 773 \pm 6 \text{ km s}^{-1}$  (internal error) for the brightest region, and  $759 \pm 21 \text{ km s}^{-1}$  for the fainter one just to its north. These compare to the consensus systemic velocity  $547 \text{ km s}^{-1}$  from NED. All lines are narrow, close to the instrumental resolution; measured FWHM values range from 1.3-1.8  $\text{\AA}$ . These observations used the B3000/R7000 grating combination, with nominal resolutions 1.7  $\text{\AA}$  in the blue and 0.9  $\text{\AA}$  at  $H\alpha$ .

The associated continuum is quite faint; even summed over all spatial pixels in the brightest knot, the continuum S/N is only 0.9 per 0.77- $\text{\AA}$  pixel at 5000  $\text{\AA}$  and 1.2 per 0.44- $\text{\AA}$  pixel near  $H\alpha$ . This limits what we can learn about associated starlight. In measuring the Balmer emission lines, we therefore consider the full range of plausible corrections for absorption in young stellar populations. While  $H\alpha$  absorption in old populations is weak, with equivalent widths near 2  $\text{\AA}$  it can be as strong as 12  $\text{\AA}$  in type A stars (Jacoby et al. 1984). Corresponding values for  $H\beta$  are 4–16  $\text{\AA}$ . Since the line emission has large equivalent widths, we include the ranges in these corrections in our uncertainties on Balmer decrement, other ratios involving these Balmer lines, and reddening. Error contributions from noise were evaluated from empty continuum regions near various emission lines. We follow Santoro et al. (2016) in converting from Balmer decrements to reddening values and  $H\alpha$  attenuation, which include both foreground Milky Way and internal contributions. Although the Milky Way absorption is significant in the direction, with  $A(H\alpha) = 0.25$  magnitude from the results of Schlafly & Finkbeiner (2011), internal attenuation is dominant in each of the three regions where we can measure the Balmer decrement.

## 3. Discussion

### 3.1. Relation to cold dust cloud

Fig. 2 overlays the  $H\alpha$  on-band image with contours of a *Spitzer*  $24\mu\text{m}$  MIPS observation described by Brookes et al. (2006); Auld et al. (2012) showed that the cloud was clearly detected

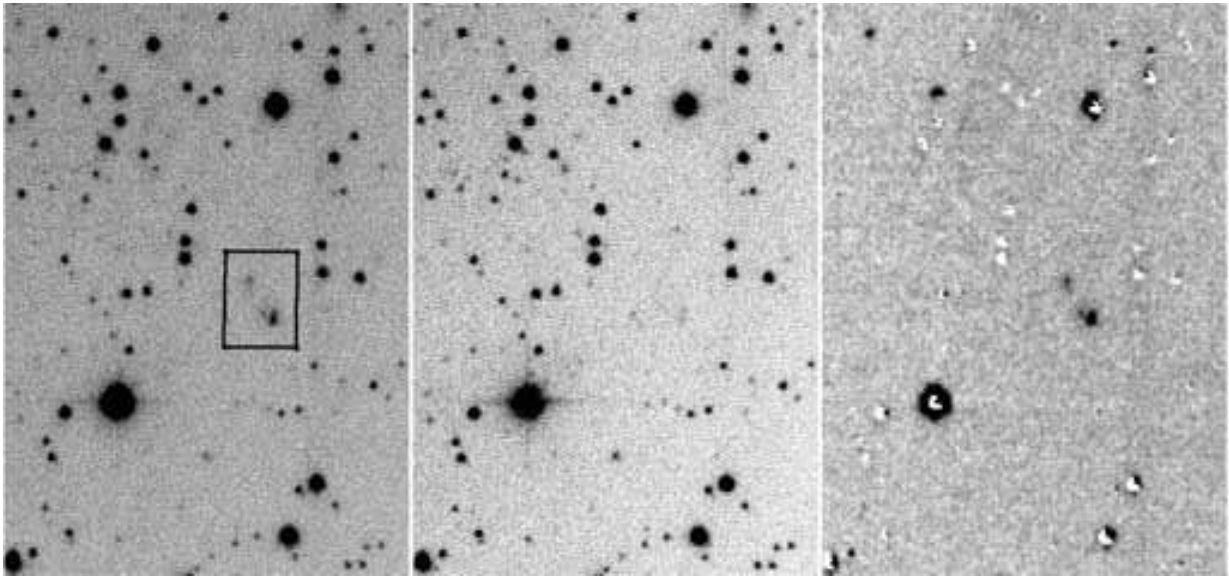


Fig. 1.— SARA  $H\alpha+[N II]$  (left) and R (center) images of the southwestern field in Centaurus A. The third panel shows a continuum-subtracted version, smoothed with a 3-pixel ( $1.2''$ ) Gaussian; approximate PSF matching was done by convolving the R images with a Gaussian of  $1.0''$  FWHM, but residuals appear in the cores of bright stars. The boxed features are essentially pure line emission. Two starlike objects to their northeast have significant residual flux in  $H\alpha$ , but may be foreground stars. Each panel spans  $178 \times 266''$ , with north at the top. The nucleus of Centaurus A lies about  $700''$  to the upper left. Faint diffuse streaks to the north in the  $H\alpha$  and difference images are scattered light from a 9th-magnitude star.

TABLE 1  
COMPONENT POSITIONS

Component	$\alpha$ (J2000)	$\delta$ (J2000)
Discrete components:		
Brightest	13 24 35.224	-43 09 09.5
North	13 24 35.186	-43 09 06.5
East	13 24 35.636	-43 09 06.9
Northeast	13 24 36.192	-43 08 52.2
Starlike emission objects:		
	13 24 41.371	-43 07 29.83
	13 24 44.032	-43 07 03.7

at this wavelength, where angular resolution is better than the longer-wavelength data from either *Spitzer* or *Herschel*. The two emission-line peaks are closely associated with the  $24\mu\text{m}$  peak locations. There are no similar  $\text{H}\alpha$  or  $24\mu\text{m}$  features within  $\approx 300''$ , leaving little doubt that these are associated physically rather than only along the line of sight.

### 3.2. Ionizing sources and star formation

To evaluate likely ionization mechanisms, we measured emission-line ratios in four spatial regions (Fig. 3), fitting Gaussian profiles and linear baselines, with results given in Table 2. These regions, selected by position and surface brightness, differ significantly in Balmer decrement  $\text{H}\alpha/\text{H}\beta$ .

All the  $[\text{S II}]$  line ratio values cluster near the low-density limit of  $I(\lambda 6717)/I(\lambda 6731)=1.43$  (mean of all values  $1.49 \pm 0.06$ ).

The location of the regions in the BPT line-ratio diagrams (Baldwin et al. 1981), using the revised dividing curves from Kewley et al. (2006), classifies all of them as photoionized by hot stars (Fig. 4). This fits with the narrow line widths measured from the WiFeS data,  $\leq 50 \text{ km s}^{-1}$ , indicating that shocks fast enough to add significantly to the ionization levels do not add significantly to the overall ionization level.

These emission regions coincide spatially with the cold dust cloud seen in *Herschel* data by Auld et al. (2012), who consider limits on the star formation set from the dust temperature and

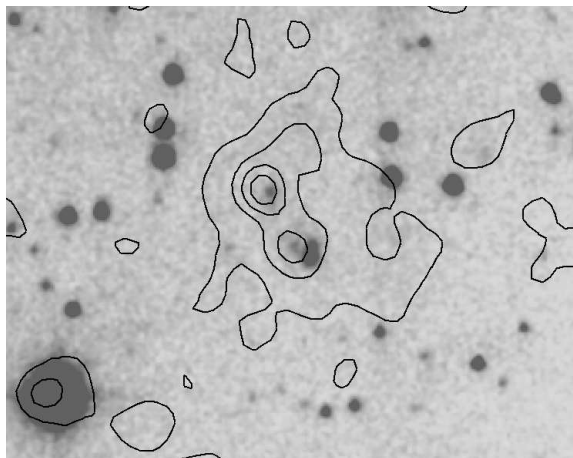


Fig. 2.— Narrowband  $\text{H}\alpha$  image as in Fig. 1, overlaid with contours from the  $24\mu\text{m}$  *Spitzer* MIPS observation. Contours are spaced at intervals  $0.10 \text{ MJy sr}^{-1}$ , spaced sparsely to show the  $\text{H}\alpha$  peaks. The area shown is  $120 \times 150''$  with north at the top.

TABLE 2  
EMISSION-LINE PROPERTIES

Quantity	Main	Main N	Diffuse	North
$F(\text{H}\alpha)$ ( $\text{erg cm}^{-2} \text{s}^{-1}$ )	$9.3 \times 10^{-15}$	$1.3 \times 10^{-15}$	$1.1 \times 10^{-15}$	$1.0 \times 10^{-15}$
$\text{H}\alpha$ EW ( $\text{\AA}$ )	$156 \pm 6$	$319 \pm 10$	$58 \pm 9$	$780 \pm 300$
[N II] $\lambda 6583/\text{H}\alpha$	$0.28 \pm 0.04$	$0.36 \pm 0.06$	$0.40 \pm 0.13$	$0.44 \pm 0.18$
[S II] $\lambda 6717/\lambda 6731$	$1.53 \pm 0.13$	$1.52 \pm 0.28$	$1.52 \pm 0.18$	$2.0 \pm 0.3$
[S II] $\lambda 6717 + 6731/\text{H}\alpha$	$0.18 \pm 0.02$	$0.27 \pm 0.07$	$0.49 \pm 0.10$	$0.25 \pm 0.07$
[O I] $\lambda 6300/\text{H}\alpha$	$0.025 \pm 0.006$	$0.018 \pm 0.002$	...	...
[O III] $\lambda 5007/\text{H}\beta$	$0.69 \pm 0.10$	$0.60 \pm 0.30$	$0.47 \pm 0.14$	...
[O II] $\lambda 3726 + 3729/[\text{O III}] \lambda 5007$	$1.6 \pm 0.5$	$< 1.0$	$4.3 \pm 1.3$	...
$\text{H}\alpha/\text{H}\beta$	$7.0 \pm 0.8$	$10.8 \pm 2.7$	$5.1 \pm 0.9$	...
$E_{B-V}$	$0.84 \pm 0.11$	$1.25 \pm 0.23$	$0.54 \pm 0.1$	...
$A(\text{H}\alpha)$	$2.10 \pm 0.18$	$3.14 \pm 0.51$	$1.35 \pm 0.40$	...
$L(\text{H}\alpha)$ ( $\text{erg s}^{-1}$ )	$1.1 \times 10^{38}$	$3.8 \times 10^{37}$	$5.7 \times 10^{36}$	$> 2.0 \times 10^{36}$

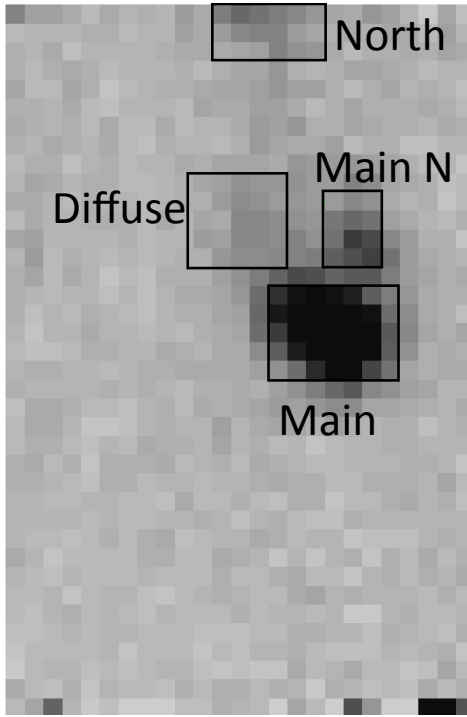


Fig. 3.— Monochromatic  $\text{H}\alpha$  image summed across the line’s emission profile from the WiFeS data cube, spanning  $24 \times 36''$  with north at the top. The regions summed in Table 2 are indicated.

(lack of) associated UV sources. Their highest allowed SFR is set from the  $24\mu\text{m}$  flux,  $0.00012 \text{ M}_{\odot} \text{ year}^{-1}$ . The GALEX-based near- and far-UV limits are much lower ( $< 2 \times 10^{-4}$  and  $< 5 \times 10^{-5} \text{ M}_{\odot} \text{ year}^{-1}$  respectively), indicating that any associated population of young stars must be obscured from our point of view.

As a star-forming region, the line emission we detect suggests that this object is modest in scale, with an  $\text{H}\alpha$  luminosity close to  $10^{38} \text{ ergs s}^{-1}$ . This is a few times greater than that of the Orion Nebula M42, requiring only a few ionizing stars ( $< 10$ ). To compare with star-formation rates in other environments, we follow Kennicutt et al. (2007), using estimating SFR from a linear combination of  $\text{H}\alpha$  and  $24\mu\text{m}$  luminosities, as calibrated for disk H II regions in M51. For the entire southwest complex in Centaurus A, this conversion gives a modest increase in effective  $\text{H}\alpha$  luminosity, and a total SFR  $1.3 \times 10^{-3} \text{ M}_{\odot} \text{ year}^{-1}$  (for a Salpeter initial-mass function). This SFR is an order of magnitude greater than the  $24\mu\text{m}$  limit from Auld et al. (2012), and correspondingly larger than their UV limits. This difference makes sense if the ionizing stars (presumably in clusters) are largely obscured along our line of sight, but the  $24\mu\text{m}$  flux is still interestingly low to be associated with even a few ionizing stars. One can, for example, picture a geometry in which the dust blocks optical and UV light over a small solid angle about the stars, but

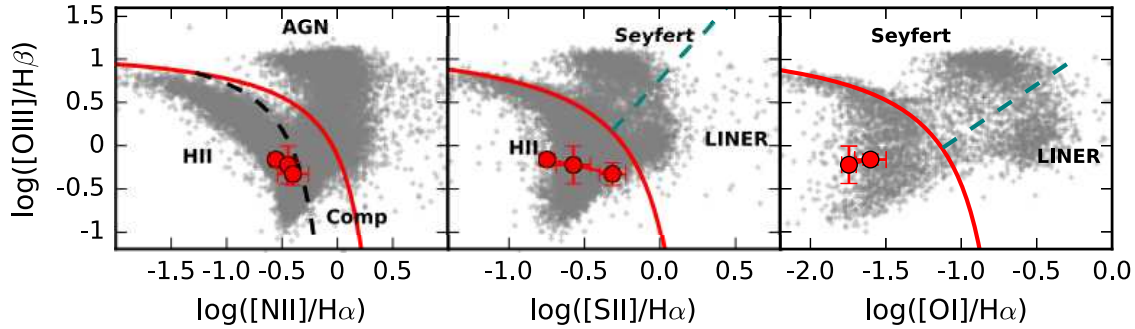


Fig. 4.— Emission-line diagnostic diagrams from Baldwin et al. (1981) and Veilleux & Osterbrock (1987). Panels show  $\log([\text{O III}]/\text{H}\beta)$  vs. (left to right)  $\log([\text{N II}]/\text{H}\alpha)$ ,  $\log([\text{S II}]/\text{H}\alpha)$ , and  $\log([\text{O I}]/\text{H}\alpha)$ , with classification boundaries from Kewley et al. (2006). Grey points show all SDSS DR12 galaxies with strong emission lines ( $\text{SNR} > 5$ ; Thomas et al. 2013). Red points show line ratios of the measured regions listed in Table 2.

still hides them from our direction.

For individual star-forming regions, the relation between long-term star-formation rate and tracers of massive stars, such as  $\text{H}\alpha$ , has a strong stochastic element. For example, using the stellar-atmosphere results from Vacca et al. (1996) and Sternberg et al. (2003) as in Gil de Paz et al. (2005) shows that the expected  $\text{H}\alpha$  luminosities from nebulae completely encompassing the star range from  $2 \times 10^{36} \text{ erg s}^{-1}$  at spectral type B0 to  $10^{38} \text{ erg s}^{-1}$  at O3. The entire ionizing flux in this complex could be provided by the equivalent of 9 O7 stars, so small-number statistics would change the emission-line output strongly as individual stars are formed and evolve. Even so, there may be more to learn; the limits on IR emission from Auld et al. (2012) are quite low in comparison to the SFR rate inferred from  $\text{H}\alpha$  emission.

The associated dust cloud matches one of the two regions in the H I “shells” of Centaurus A where Charmandaris et al. (2000) detected CO emission, implying a typical  $\text{H}_2/\text{H I}$  ratio near unity and consistent with conditions for star formation in the inner regions of spirals. With an estimated  $\text{H}_2$  mass of  $2 \times 10^7 M_\odot$  and linear scale  $\approx 0.5 \text{ kpc}$ , this would be either an exceptionally large giant molecular cloud or a collection of more

usual clouds (noting that geometrically it may not be easy to distinguish these cases). Under these conditions, it would be common for parts of a “blister” H II region to be highly obscured in the optical unless viewed face-on, which fits with the low UV limits on radiation from young stars.

In  $\text{H}\alpha$  luminosity and Balmer decrement, these star forming regions are similar to those found embedded in the northeastern filaments (in what is sometimes known as the “necklace” structure) by Santoro et al. (2016). In comparison with the Santoro et al. (2016) regions, these are comparable in scale and observed luminosity, although perhaps more luminous when dereddened (Fig. 5). We might speculate that in both cases, interaction with a central outflow Neff et al. (2015) has compressed ambient H I to trigger star formation, but that the southwestern structure lacks the additional ingredients of a direct view of the AGN and a collimated radio jet which enhance both effects in the gas kinematics and ionization on the “jet” side.

#### 4. Summary

We have described a set of optical emission-line regions found 12 kpc to the southwest of the nucleus of Centaurus A, closely coincident with

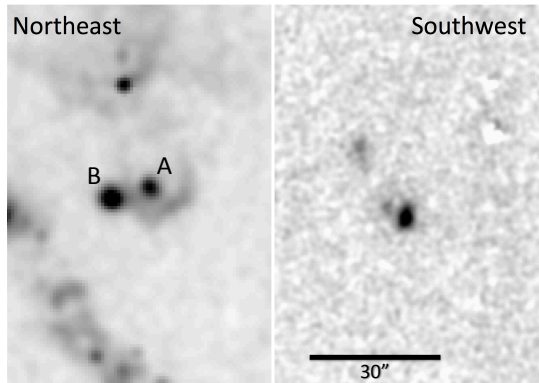


Fig. 5.— Comparison of the newly observed star-forming regions (right panel) with the H II regions A and B found in the northeastern emission-line jet by Santoro et al. (2016) (left). The additional filamentary features on the northwest side are ionized by the AGN, either photoionized or via interaction with the radio jet. Both panels show H $\alpha$  emission and are at the same angular and intensity scales. The jet region was imaged using the ESO/MPI 2.2m telescope as described by Keel (1989).

dust and gas structures previously reported. The emission-line ratios as well as UV and FIR properties are well accommodated as a set of normal H II regions, photoionized by only a few OB stars.

Even in a system as disturbed as Centaurus A, this is a distant place to find apparently normal H II regions. Fig. shows the location superimposed on an H $\alpha$  image of the inner regions, where the rich distribution of star-forming regions is strongly confined to the warped remnant disk, within a radius of 212'' (3.8 kpc). Charmandaris et al. (2000) suggest that an outflow from the central regions of the system has played a role in compressing gas (possibly concentrated dynamically in a way similar to the stellar shells) so as to trigger such distant star formation. On this basis, we might speculate that star formation can be triggered by a broad outflow (driven either by the AGN or strong star formation in the inner disk), but the southwest region lacks the additional factors producing the rich optical emission along the north jet. This difference could mean that there is no collimated radio jet on this side, that the southwestern cloud of gas and dust is not in the right place to be ionized by AGN radiation, or that the AGN radiation does not escape effectively on this side.

The IFU spectroscopy was facilitated by a Twitter interaction between two of the authors. This research has made use of the NASA/IPAC Infrared Science Archive, which is operated by the Jet Propulsion Laboratory, California Institute of Technology, under contract with the National Aeronautics and Space Administration. This research has made use of NASA's Astrophysics Data System Bibliographic Services. Support for AMM is provided by NASA through Hubble Fellowship grant HST-HF2-51377 awarded by the Space Telescope Science Institute, which is operated by the Association of Universities for Research in Astronomy, Inc., for NASA, under contract NAS5-26555. Funding for the Sloan Digital Sky Survey IV has been provided by the Alfred P. Sloan Foundation, the U.S. Department of Energy Office of Science, and the Participating Institutions. SDSS acknowledges support and resources from the Center for High-Performance Computing at the University of Utah. The SDSS web site is [www.sdss.org](http://www.sdss.org). SDSS is managed by the Astrophysical Research Consortium for the Participating Institutions of



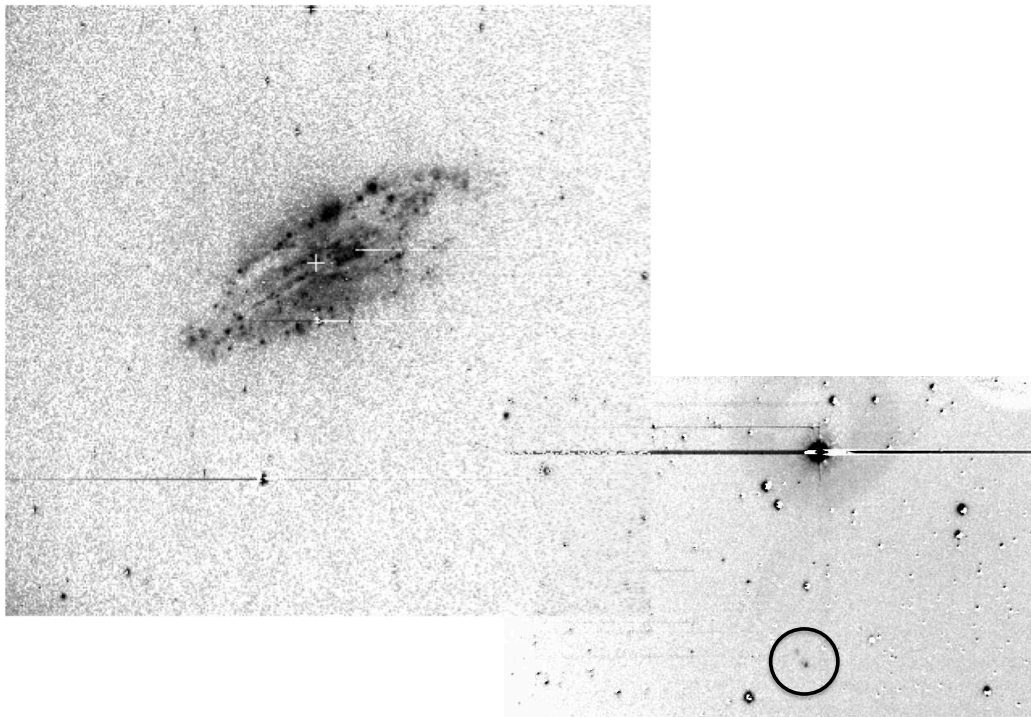


Fig. 6.— SARA  $H\alpha+[N II]$  image mosaic showing the newly described H II regions in a wider context including the core of Centaurus A. The continuum has been subtracted using an  $R$ -band image, leaving some residuals around bright stars. The prominent disk of emission around the nucleus extends to a radius  $212''$ , while the southwest knots are  $700''$  away.

the SDSS Collaboration including the Brazilian Participation Group, the Carnegie Institution for Science, Carnegie Mellon University, the Chilean Participation Group, the French Participation Group, Harvard-Smithsonian Center for Astrophysics, Instituto de Astrofísica de Canarias, The Johns Hopkins University, Kavli Institute for the Physics and Mathematics of the Universe (IPMU) / University of Tokyo, Lawrence Berkeley National Laboratory, Leibniz Institut für Astrophysik Potsdam (AIP), Max-Planck-Institut für Astronomie (MPIA Heidelberg), Max-Planck-Institut für Astrophysik (MPA Garching), Max-Planck-Institut für Extraterrestrische Physik (MPE), National Astronomical Observatories of China, New Mexico State University, New York University, University of Notre Dame, Observatorio Nacional / MCTI, The Ohio State University, Pennsylvania State University, Shanghai Astronomical Observatory, United Kingdom Participation Group, Universidad Nacional Autónoma de México, University of Arizona, University of Colorado Boulder, University of Oxford, University of Portsmouth, University of Utah, University of Virginia, University of Washington, University of Wisconsin, Vanderbilt University, and Yale University.

Facilities: SARA, ATT, Spitzer, ESO

## REFERENCES

- Auld, R., Smith, M. W. L., Bendo, G., et al. 2012, *MNRAS*, 420, 1882
- Baldwin, J. A., Phillips, M. M., & Terlevich, R. 1981, *PASP*, 93, 5
- Blanco, V. M., Graham, J. A., Lasker, B. M., & Osmer, P. S. 1975, *ApJ*, 198, L63
- Brookes, M. H., Lawrence, C. R., Keene, J., et al. 2006, *ApJ*, 646, L41
- Charmandaris, V., Combes, F., & van der Hulst, J. M. 2000, *A&A*, 356, L1
- Crnojević, D., Ferguson, A. M. N., Irwin, M. J., et al. 2013, *MNRAS*, 432, 832
- Crockett, R. M., Shabala, S. S., Kaviraj, S., et al. 2012, *MNRAS*, 421, 1603
- Dopita, M., Hart, J., McGregor, P., et al. 2007, *Ap&SS*, 310, 255
- Evans, I. N., & Koratkar, A. P. 2004, *ApJ*, 617, 209
- Gil de Paz, A., Madore, B. F., Boissier, S., et al. 2005, *ApJ*, 627, L29
- Graham, J. A., & Price, R. M. 1981, *ApJ*, 247, 813
- Jacoby, G. H., Hunter, D. A., & Christian, C. A. 1984, *ApJS*, 56, 257
- Junkes, N., Haynes, R. F., Harnett, J. I., & Jauncey, D. L. 1993, *A&A*, 269, 29
- Keel, W. C. 1989, European Southern Observatory Conference and Workshop Proceedings, 32, 427
- Keel, W. C., Oswalt, T., Mack, P., et al. 2017, *PASP*, 129, 015002
- Kennicutt, R. C., Jr., Calzetti, D., Walter, F., et al. 2007, *ApJ*, 671, 333
- Kewley, L. J., Groves, B., Kauffmann, G., & Heckman, T. 2006, *MNRAS*, 372, 961
- Landolt, A. U. 2009, *AJ*, 137, 4186
- Lang, D., Hogg, D. W., Mierle, K., Blanton, M., & Roweis, S. 2010, *AJ*, 139, 1782
- McKinley, B., Tingay, S. J., Carretti, E., et al. 2017, arXiv:1711.01751
- Morganti, R., Robinson, A., Fosbury, R. A. E., et al. 1991, *MNRAS*, 249, 91
- Neff, S. G., Eilek, J. A., & Owen, F. N. 2015, *ApJ*, 802, 88
- Osmer, P. S. 1978, *ApJ*, 226, L79
- Peterson, B. A., Dickens, R. J., & Cannon, R. D. 1975, Proceedings of the Astronomical Society of Australia, 2, 366
- Rejkuba, M., Minniti, D., Courbin, F., & Silva, D. R. 2002, *ApJ*, 564, 688
- Santoro, F., Oonk, J. B. R., Morganti, R., & Oosterloo, T. 2015, *A&A*, 574, A89
- Santoro, F., Oonk, J. B. R., Morganti, R., Oosterloo, T. A., & Tadhunter, C. 2016, *A&A*, 590, A37

- Schlafly, E. F., & Finkbeiner, D. P. 2011, *ApJ*, 737, 103
- Sternberg, A., Hoffmann, T. L., & Pauldrach, A. W. A. 2003, *ApJ*, 599, 1333
- Sutherland, R. S., Bicknell, G. V., & Dopita, M. A. 1993, *ApJ*, 414, 510
- Thomas, D., Steele, O., Maraston, C., et al. 2013, *MNRAS*, 431, 1383
- Tully, R. B., Courtois, H. M., Dolphin, A. E., et al. 2013, *AJ*, 146, 86
- Tully, R. B., Libeskind, N. I., Karachentsev, I. D., et al. 2015, *ApJ*, 802, L25
- Vacca, W. D., Garmany, C. D., & Shull, J. M. 1996, *ApJ*, 460, 914
- Veilleux, S., & Osterbrock, D. E. 1987, *ApJS*, 63, 295